THE JOURNAL OF PHYSICAL CHEMISTRY A

ARTICLE

pubs.acs.org/JPCA

CO_2 in Solid Para-Hydrogen: Spectral Splitting and the $CO_2\cdots(o\text{-}H_2)_n$ Clusters

Jun-He Du, Lei Wan, Lei Wu, Gang Xu, Wen-Ping Deng, An-Wen Liu, Yang Chen, and Shui-Ming Hu*

Hefei National Laboratory for Physical Sciences at Microscale, Department of Chemical Physics, University of Science and Technology of China, Hefei, 230026 China

ABSTRACT: Complicated high-resolution spectral structures are often observed for molecules doped in solid molecular hydrogen. The structures can result from miscellaneous effects and are often interpreted differently in references. The spectrum of the ν_3 band of CO_2 in solid para-H_2 presents a model system which exhibits rich spectral structures. With the help of the potential energy simulation of the CO_2 molecule doped in para-hydrogen matrix, and extensive experiments with different CO_2 isotopologues and different ortho-hydrogen concentrations in the matrix, the spectral features observed in p-H_2 matrix are assigned to the $CO_2\cdots(o\text{-}H_2)_n$ clusters and also to energy level splitting that is due to different alignments of the doped CO_2 molecules in the matrix. The assignments are further supported by the dynamics analysis and also by the spectrum recorded with sample codoped with O_2 which serves as catalyst transferring o-H_2 to p-H_2 in the matrix at 4 K temperature. The observed spectral features of CO_2/pH_2 can potentially be used as an alternative readout of the temperature and orthohydrogen concentration in the solid para-hydrogen.

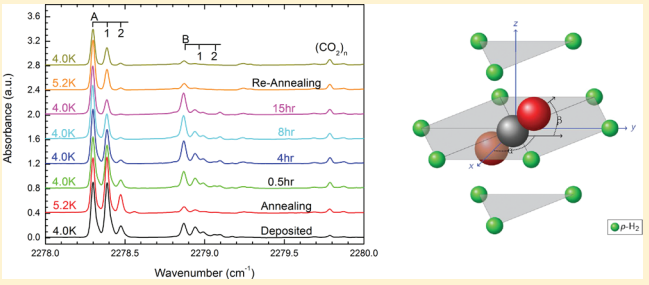

1. INTRODUCTION

The matrix shift and the matrix splitting observed in matrix isolation spectroscopy provide a measure of the intermolecular interactions between the guest and the host molecules. Interactions between guest dopants and host rare gas solids are usually characterized with band shift and line broadening. However, in the case of solid molecular hydrogen (SMH) matrix, complicated spectroscopic structure can often be found for a single vibrational band of the dopant molecule. Because of the unique quantum character of SMH, such a structure has attracted more and more interest in recent years.

The spectral structures can simply come from the rotation of the doped molecules in SMH matrix. Quite a few molecules have been observed rotating almost freely in solid para-hydrogen, including but not limited to methane,[1,2] H_2O,[3,4] CO,[5] and HCl.[6] However, it does not apply for some other molecules with relatively smaller rotational constants in case that the rotation of the guest molecules is hindered because of the presence of matrix field. Fajardo et al. presented the ro-vibrational spectra of CO in SMH and discussed the crystal field induced spectral features.[5] The complicated spectral structure may also result from the dopant-(*ortho*-$H_2)_n$ clusters in solid para-hydrogen. Because of the nonspherical nature of the wave function of *ortho*-H_2 (o-H_2, $J = 1$ at low temperature), the o-H_2 molecule will have stronger interactions with the dopant molecules than that for the *para*-H_2 (p-H_2, $J = 0$ at low temperature) molecule. As a result, although the concentration of o-H_2 is very low (typically less than 0.1%) in many experiments using p-H_2 as matrix host, through spin and rotation exchange process between nearby p-H_2 and o-H_2 molecules, dopant-$(o\text{-}H_2)_n$ clusters have been observed accumulating in the matrix at very low temperature. Spectra of o-H_2 clustering with various dopant molecules have been observed, including *trans*-formic acid,[7] CH_3F,[8−10] Cl, and H atoms.[11] Lorenz and Anderson studied the ν_3 band of N_2O in solid para-hydrogen and investigated the spectroscopy of N_2O-$(o\text{-}D_2)_N$ and N_2O-$(HD)_N$ clusters.[12] They also mentioned the reversible spectral structures in the spectrum of N_2O in bulk solid para-hydrogen. Such structures exhibit slow changes (in hours) at very low temperature (1.7−4.8 K). We have extended the study of N_2O in solid para-H_2 to the overtones as high as $5\nu_1$.[13]

Although it is still quite difficult to interpret quantitatively the spectrum of doped SMH system, the rich spectroscopy features provide a unique platform to look into the dynamics of such van der Waals force dominated molecular systems. Here, we will present the study of CO_2 doped in p-H_2 matrix. Because CO_2 is a simplest symmetric linear triatomic molecule, and because of its importance in various studies, its spectrum has been extensively studied and so far has been well understood. The matrix isolation spectroscopy of CO_2 has been reported in solid N_2,[14,15] O_2,[16] Ne,[17] Ar,[14,15,18] Kr,[19] *para*-H_2,[20] and helium droplet.[21] However, as will be discussed later, the spectrum of CO_2 doped in solid para-hydrogen shows surprisingly complicated features, and it

Received: September 14, 2010
Revised: December 8, 2010
Published: January 25, 2011

provides an excellent example to investigate the interactions and dynamics in the solid para-hydrogen. The high-resolution study of CO_2 doped in *para*-H_2 matrix by Tam et al. mentioned the complicated spectral features of the ν_3 band and proposed that possible multiple geometry of doped CO_2 taking multiple H_2 vacancies in the crystal may be accounted for in the spectral structures. However, as will be presented here, the well repeatable and reversible spectral features observed in our study imply that the spectrum is a result of delicate structure and dynamics instead of a result of crystal defects. Simulation of the potential of CO_2 isolated in solid *p*-H_2, experimental results, and discussions will be presented in following sections.

2. SIMULATION OF THE POTENTIAL SURFACE OF CO_2 DOPED IN PARA-HYDROGEN

Before trying to understand the spectrum and dynamics of CO_2 doped solid para-hydrogen, we took a simple simulation of the interactions on the basis of the available CO_2-H_2 potential. Such potential has been well established on the basis of the experimental[22] and theoretical[23,24] studies of the CO_2-H_2 complex in the gas phase. In principle, the doping potential of CO_2 molecule in solid hydrogen can be derived from the two-body potential of CO_2-H_2 and that of H_2-H_2 provided that only the two-body interactions are important. However, the local distortion of the crystal around the doped CO_2 molecule may also lead to a complicated treatment which may be sensitive to the two-body potentials and which may be beyond the view of the present paper. In the present study, we are more concentrating on the potential analysis to answer a few fundamental questions which will be directly related to the structure and dynamics revealed from the spectrum: (1) Does the CO_2 molecule rotate in the solid H_2 crystal? (2) If the rotation is hindered, what will be the most preferred (with lowest potential energy) orientations of the molecule? In this case, we preferred a simplified simulation of CO_2 in solid *para*-H_2 matrix using the CO_2-H_2 complex potential given by Ran et al.[24]

As confirmed by both the experimental[22] and theoretical[23,24] results, the equilibrium distance between the CO_2 and the H_2 molecules in the CO_2-H_2 complex is about 3.5 Å, which is a little less than the distance (3.8 Å) between two nearby H_2 molecules in solid H_2. In this case and also for simplicity, we just consider the single-substituted structure in which the CO_2 molecule simply substitutes one H_2 molecule in the crystal. The structure is shown in Figure 1.

Apparently, the CO_2 molecule may have different orientations in the crystal. Ran et al.'s two-body potential is applied to calculate the potential of each probable orientation. Since the force between the CO_2 and the H_2 molecules decreases rapidly when the distance between the molecules goes up, only the nearest H_2 molecules around CO_2 are included in the simulation. For simplicity, the 12 nearest *p*-H_2 molecules are fixed on their equilibrium positions in the *p*-H_2 crystal. The CO_2 orientation potential has been calculated with the sum of the two-body potential of the CO_2 molecule and each of the 12 nearest *p*-H_2 molecules. As a result, the orientation potential is a function of the position of the CO_2 molecule in the crystal (x, y, z) and the alignment of the O−C−O molecule which can be described with two angles α and β. x, y, and z are the Cartesian coordinates of the center of the CO_2 molecule, β is the angle between the CO_2 molecule and the xy plane, and α is the angle between the x axis and the projection of CO_2 on the xy plane. The calculated

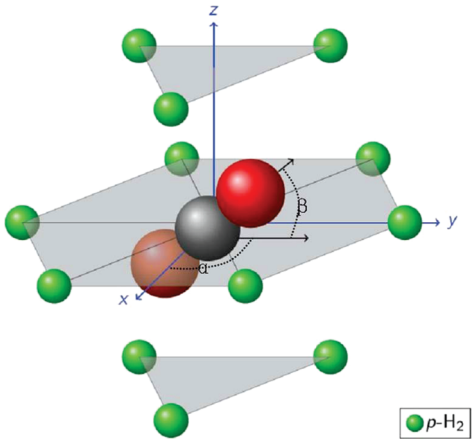

Figure 1. Configuration of the single-substituted CO_2 in hcp crystal of solid H_2. β is the angle between the CO_2 molecule and the xy plane. α is the angle between the x axis and the projection of CO_2 on the xy plane.

orientation potential shows that one of the most optimized orientations of the CO_2 molecule is at $x = 0.6$ Bohr, $y = z = 0$, with alignment angles $\alpha = 0°$ and $\beta = 38.7°$, while the central position with $x = y = z = 0$ gives a potential energy of about 32 cm^{-1} higher. Figure 2a shows the orientation potential for each (x, y) position with z value fixed to zero and with α, β angles at the optimized values.

As shown in Figure 2a, there are three potential energy minima around the central position. A pathway can be drawn connecting these minima, and its projection on the $z = 0$ surface is also shown in Figure 2a. This pathway has the lowest barrier between the nearby minima. The calculated optimized alignment angles α, β and the potential energies along the pathway are shown in the same figure as panels b, c, and d, respectively. This pathway is the classical trajectory that the doped molecule undergoes when traveling from one equilibrium orientation to another. In Figure 2d, the barrier between different potential minima is only a few wavenumbers. In this case, tunneling between these orientations should be significant.

To find out wether or not the CO_2 molecule can rotate in solid H_2, we calculated the potential function of the CO_2 molecule at different alignments (with different α and β angles). The calculated potential with the position fixed at $x = y = z = 0$ is shown in Figure 3. For symmetry reason, only the part of $\alpha = 0-60°$ and $\beta = 0-90°$ is given. As shown in the figure, the potential minimum locates at $\alpha = 0°$ (or 60°), $\beta = 38.7°$. The tunneling from $\alpha = 0°$ to $\alpha = 60°$ without changing the β angle (libration of CO_2 along the z axis) has a barrier of about 20 cm^{-1}. The motion from $\beta = 38.7°$ to $\beta = -38.7°$ without changing the α angle (rotation with an axis in the xy plane) has a barrier of about 60 cm^{-1}. Since the barrier height is a few hundred times that of the rotational constant of the CO_2 molecule ($\sim$0.4 cm^{-1}), the molecules are unlikely able to rotate in the crystal but are likely to tunnel among different alignments. According to the group theory for matrix-isolated molecules reported by Miller and Decius,[25] for the linear molecule like CO_2 in a crystal field with D_{3h} symmetry, as the case for an hcp crystal of *p*-H_2, the symmetry of the librational states will be A_1 for the ground state and E for the first excited state. In this case, each of the vibrational states of CO_2 consists of a series of librational levels. The energy splitting depends on the tunneling barrier height and also on the rotational constant of the doped CO_2 molecule.

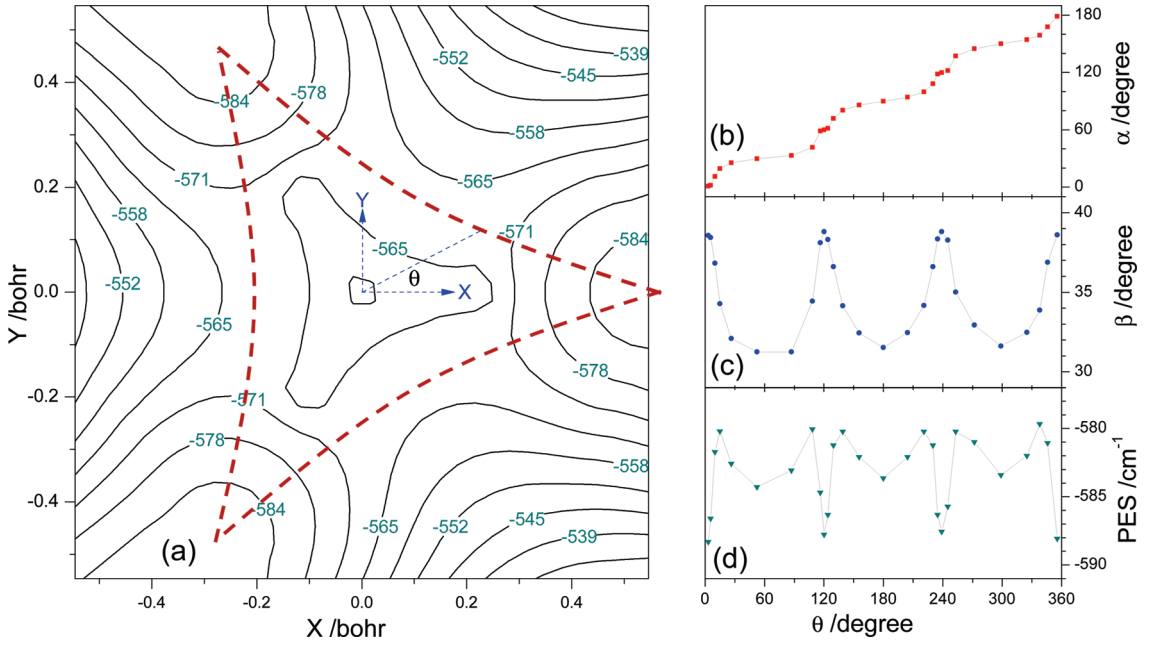

Figure 2. (a) Contour plot of the orientation potential energies of CO_2 molecule in solid H_2 (in cm^{-1}). The z value was fixed to zero and the alignment angles (α and β) were at optimized values. There is a classical pathway connecting three global minima on the potential energy surface. The projection of the trajectory on the $z = 0$ surface is also shown in panel a. The calculated optimized alignment angles α, β and the potential energy along the pathway are shown in panels b, c, and d, respectively.

Although the simulation of the potential surface given earlier should be regarded qualitatively rather than quantitatively, we can still draw a few conclusions from the simulation: (1) The guest CO_2 molecule can hardly rotate in solid p-H_2, but some libration motion may be allowed. (2) There are quite a few equilibrium orientations of the CO_2 molecule that are allowed in solid p-H_2. These orientations include different alignments (α and β) or positions (x, y, z). Tunneling between these orientations will lead to additional energy splitting of the ground and vibrationally excited states of CO_2.

3. EXPERIMENTAL DETAILS

The experimental setup is close to those used in our previous studies.[13,26] We just give a brief description here. A converter filled with $Fe(OH)_3$ catalyst was applied to convert normal H_2 to p-H_2. The catalyst was filled in a 1.6 m long OFHC tube which is attached tightly on the cold head of a cryostat (Sumitomo 205D). During converting, the converter temperature is monitored with a diode sensor (DT-470) and is controlled with a feed-back temperature controller (Lake Shore 331S). The converting temperature is maintained at 14−15 K. In this way, hydrogen gas with *ortho*-H_2 concentration lower than 0.1% can be obtained.

Direct deposition method is used to prepare solid molecular hydrogen film as described by Fajardo and Tam.[27] A helium close-cycle cryogenerator (Janis SHI-4−5) is used to maintain temperature as low as 3.5 K at its second cryogenic stage. The temperature is detected with a silicon diode sensor and is controlled with a controller (Lakeshore 331S) using a feedback loop and a heating resistance wires installed on the cold stage. A BaF_2 base plate used for film deposition is fixed in an OFHC copper frame which is attached to the second cryogenic stage tightly. The cold head is inserted into the sample chamber of a

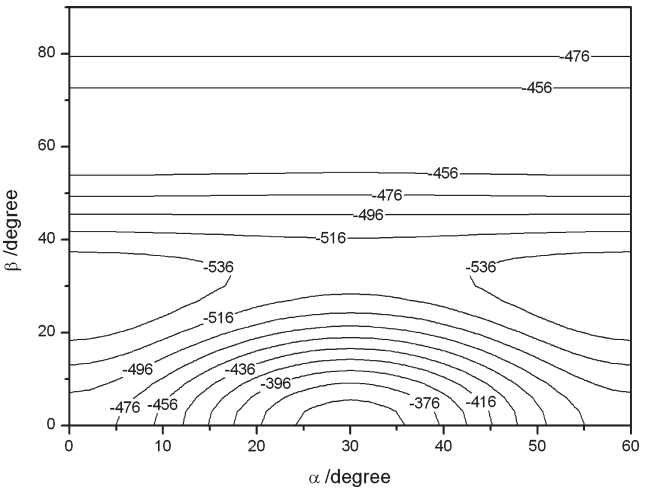

Figure 3. Contour plot of the potential energy (in cm^{-1}) of CO_2 doped in p-H_2 matrix with different alignments.

Fourier transform (FT) spectrometer (Bruker IFS120HR). The sample chamber is isolated from the Fourier transform interference chamber and is pumped to 10^{-5} Pa with a turbo pump. The interference chamber is also evacuated to about 40 Pa to decrease the air absorption in the spectrum. During deposition, the cold BaF_2 base plate is perpendicular to the gas inlet. The gas sample is deposited onto the base plate, and the gas flow rate is controlled by a mass flow controller (MKS 1479A). When the deposition is finished, the cryogenic cold head (together with the cold plate) will be rotated under vacuum to align the BaF_2 base plate perpendicular to the FT probing light, and the spectrum will be recorded.

Natural and isotope concentrated CO_2 samples were used in the present study. The one with natural isotopic abundance was

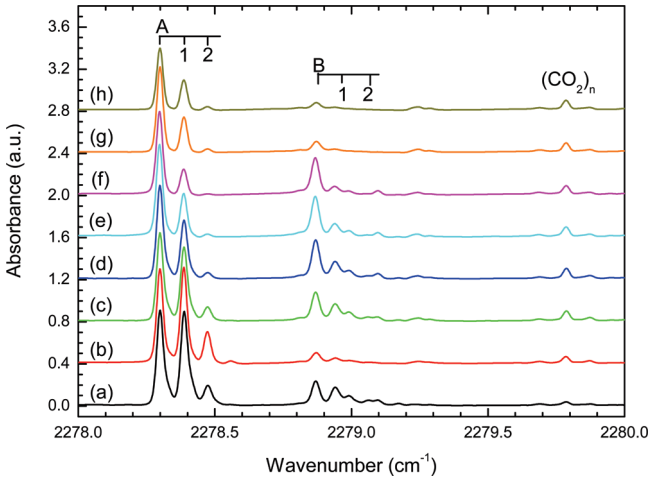

Figure 4. Fourier transform spectrum of the ν_3 band of $^{13}C^{16}O_2$ isolated in solid *para*-H_2. Spectral resolution: 0.02 cm^{-1}. The index 1, 2 shown on the figure indicates the number of *o*-H_2 molecules in the nearest neighbor of the doped CO_2 molecule. From bottom to top: (a) 4.0 K, as deposited, (b) 5.2 K, annealing, (c) 4.0 K, just after half an hour's annealing at 5.2 K, (d) 4.0 K, 4 h after the annealing, (e) 4.0 K, 8 h after the annealing, (f) 4.0 K, 15 h after the annealing, (g) 5.2 K, reannealing for half an hour, (h) 4.0 K, 1 h after the second annealing. The traces are displaced vertically for ease of presentation.

bought from Nanjing Special Gas Inc. ^{13}C enriched and ^{18}O enriched samples were purchased from Icon Services Inc. The isotopic abundance of each sample was determined by the infrared spectroscopy and also by the photoionization mass spectroscopy (PIMS) measurements. The PIMS measurement was carried out in the photochemistry end-station of National Synchrotron Radiation Laboratory (Hefei, China). Typically, a few ppm CO_2 sample was mixed with hydrogen gas before deposition. The sample gas was deposited on the cold BaF_2 plate with a typical mass flow rate of 27 mmol/h and with a duration time of about half an hour. The FT spectra were recorded at a resolution of 0.02 cm^{-1}.

4. RESULTS AND DISCUSSION

Matrix Shift and Isotopic Dependence. The measurements of different CO_2 isotopologues in solid *para*-hydrogen matrix have been carried out with isotope concentrated CO_2 samples. A total of 10 different isotopologues of CO_2 were studied: $^{12}C^{16}O_2$, $^{13}C^{16}O_2$, $^{12}C^{18}O_2$, $^{16}O^{12}C^{18}O$, $^{16}O^{12}C^{17}O$, $^{16}O^{13}C^{18}O$, $^{16}O^{13}C^{17}O$, $^{13}C^{18}O_2$, $^{17}O^{12}C^{18}O$, and $^{12}C^{17}O_2$. These isotopologues are noted as 626, 636, 828, 628, and so on, respectively. The fine features of the spectra of different CO_2 isotopologues are very similar, and a part of the ν_3 band of $^{13}C^{16}O_2$ is shown in Figure 4. The position of the leading strong line in the "A" feature (shown in Figure 4) of the ν_3 band for each CO_2 isotopologue is given in Table 1. It is used as an indicator of the matrix shift for each isotopologue. For convenience, the gas phase band centers of the ν_3 bands of all the studied isotopologues[28,29] are also given in the same table.

As a zero-order approximation, the frequency of a harmonic oscillator ω can be simply written as $\omega = (k/\mu)^{1/2}$, where k is the force field constant and μ is the reduced mass of the oscillator. Linear dependence of the oscillator frequency on the $1/(\mu)^{1/2}$ value is expected on isotopic substitution. For the ν_3 normal mode vibration of the CO_2 molecule, the reduced mass can be calculated with the normal mode mass matrix analysis,[30] and the calculated μ values of different CO_2 isotopologues are presented in Table 1. Figure 5 illustrates the *p*-H_2 matrix shifts of different CO_2 isotopologues. Excellent linear dependence can be readily seen for two groups of isotopologues. Five isotopologues with center ^{12}C are on one line and another five isotopologues with ^{13}C are on another line. If the Born−Oppenheimer approximation remains effective, the force constant should be the same for different isotopologues, and even the CO_2-H_2 interactions have been taken into account. The anomalous isotope shifts can be explained by the following: if the nearby H_2 molecules are kinetically involved in the CO_2 vibrations, as the H_2 molecules adhere to the stretching motion of the central CO_2 molecule, there will be additional corrections to the reduced mass and also probably to the anharmonicity of the vibration which are both more sensitive to the center carbon atomic mass.

ν_3 Band Structure. A few groups of lines spread within a few wavenumebrs in the CO_2 ν_3 band region. The spectral features are almost the same for different CO_2 isotopologues. Figure 4 shows the ν_3 band of $^{13}C^{16}O_2/p$-H_2 measured at different times before and after annealing. The *ortho*-H_2 concentration in the matrix is estimated to be 0.15%. Two band features marked with A and B on the figure have reversible character before and after annealing. The irreversible feature at the higher spectral part (near 2279.8 cm^{-1} for $^{13}C^{16}O_2/p$-H_2) is assigned to aggregated $(CO_2)_n$ clusters. As shown in Figure 4, the group B lines dropped quickly when the crystal temperature was raised to 5.2 K during annealing and slowly went up when the temperature decreased again to 4.0 K after annealing. To illustrate such a slow relaxation process at 4.0 K, the spectrum has been continuously measured for over 15 h. The evolution of the relative intensity of the B line to the A line is shown in Figure 6. A single exponential fitting shows that the relaxation time is about 2.2 h.

There can be several explanations of the observed spectral splitting. The leading lines of the A and B features have also been observed by Tam and Fajardo,[20] and it is proposed that the features are related to different trapping sites on the basis of single-, double-, and triple-substitutional vacancies in solid *p*-H_2. However, as discussed in the simulation section of the present work, and also because of the reversible character of the spectral feature, it is more likely that the CO_2 molecule will simply substitute single *p*-H_2 molecule in the crystal. The reversibility of the feature also excludes the explanation with unstable trapping sites of the CO_2 molecule in the crystal. Other explanations may include guest molecule aggregation, rotation, or crystal defects. The possibility of aggregation can be easily excluded since the features remain almost the same with the CO_2 concentration in the sample varying from several to hundreds ppm. It is also unlikely to be from guest molecule rotations though the reversible nature of the spectral features implies a population distribution very sensitive to the temperature. As shown in Figure 3 and as concluded in our simulation, the rotation of the CO_2 molecule should be hindered by the presence of surrounding *p*-H_2 molecules. We cannot fully exclude the possibility that the spectral splitting comes from miscellaneous crystal defects around the guest molecule or from the rearrangement of the neighboring hydrogen molecules, but the reason for the temperature dependence is inexplicit and we do not have further observation to support this explanation. Here, we tend to assume that the spectral feature may come from the energy level splitting because of multiple alignments of the doped CO_2 molecule. As we have discussed in section 2, there are a few different CO_2

Table 1. ν_3 Band Shifts in Solid p-H_2 of Different Isotopologues of Carbon Dioxide

isotope[a]	G_v[b]	ν_{pH_2}	Δ[c]	μ[d]	isotope	G_v	ν_{pH_2}	Δ	μ
626	2349.143	2343.817	−5.325	4.36326	636	2283.487	2278.300	−5.187	4.62265
627	2340.014	2334.717	−5.297	4.39831	637	2274.087	2268.929	−5.158	4.66197
628	2332.112	2326.843	−5.270	4.42912	638	2265.971	2260.839	−5.132	4.69651
728	2322.436	2317.192	−5.244	4.46678	738	2255.954	2250.851	−5.103	4.73898
828	2314.048	2308.831	−5.217	4.49995	838	2247.291	2242.214	−5.077	4.77636

[a] Index of different isotopologues, 626 for $^{16}O^{12}C^{16}O$, 627 for $^{16}O^{12}C^{17}O$, and so on. [b] Gas-phase values from refs 28 and 29. [c] Solid p-H_2 matrix shift, $\Delta = \nu_{pH_2} - G_v$. [d] Reduced mass of the ν_3 antisymmetric stretching mode.

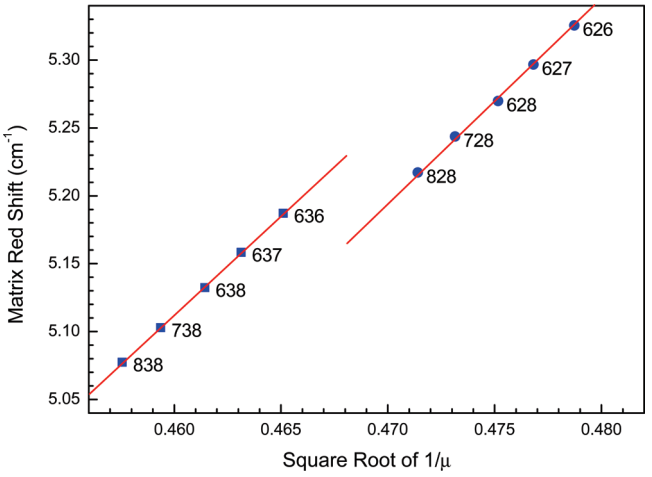

Figure 5. The ν_3 band shifts in solid p-H_2 of different isotopologues of carbon dioxide. The CO_2 isotopologues are indexed as 628 for $^{16}O^{12}C^{18}O$, 636 for $^{16}O^{13}C^{16}O$, etc.

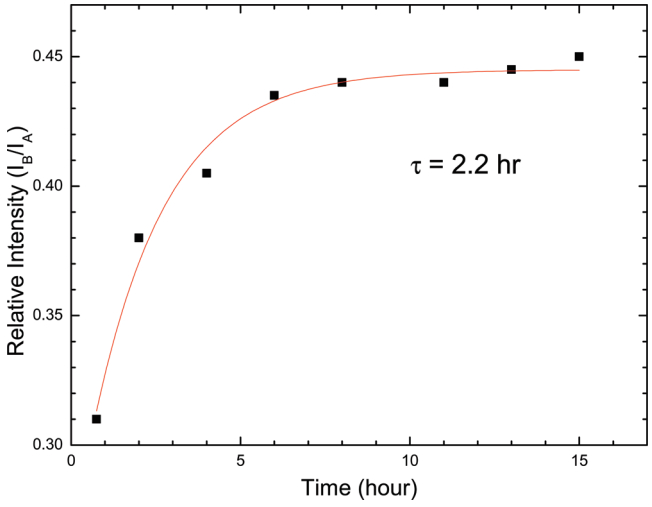

Figure 6. Time evolution of the relative intensity of line B over line A measured at 4.0 K after the crystal has been annealed at 5.2 K.

alignments in the crystal. The presence of tunneling will lead to energy splitting among degenerated energy levels. We assign the A and B spectral features to such a splitting effect. In this case, when the temperature changes, the populations on different sublevels will change accordingly, and it leads to a different intensity ratio of the A and B lines. According to the spectra, we can conclude that the A line is related to sublevels with higher energy which is less populated at low temperature but is more populated at relatively higher temperature. It is also consistent with the observation given in ref 20, which shows that the A line is relatively stronger at 4.8 K but is weaker at 2.4 K. At the present stage, it is still hard to quantitatively interpret the relative line intensity and the long relaxation time shown in Figure 6.

Absorption Spectral Features because of CO_2-(o-H_2)$_n$ Clusters. As shown in Figure 4, each of the A and B features actually consists of a group of lines. To have a further insight into this feature, we measured the spectrum with different concentrations of ortho-hydrogen by mixing a controlled amount of normal hydrogen with the para-hydrogen gas before the deposition. Figure 7 shows the results. All the spectra were measured at 4.4 K after the film was annealed at 5.2 K for 30 min. It is clearly shown that when the concentration of ortho-hydrogen increases, the band weight center moves to the blue side. In this way, we assign the observed features to the $CO_2\cdots(o\text{-}H_2)_n$ clusters in solid p-H_2. The distances between the nearby $CO_2\cdots(o\text{-}H_2)_n$ (n = 0, 1, 2) lines in the A features shown in Figure 4 (for $^{13}C^{16}O_2$) and in Figure 7 (for $^{12}C^{16}O_2$) are all about 0.09 cm^{-1}. This value is very close to the experimental ν_3 band shift between the $CO_2\cdots p$-H_2 and $CO_2\cdots o$-H_2 complexes which is 0.10 cm^{-1} given in refs 22 and 23. Such agreement also confirms the assignments.

It is interesting that for statistical reason, CO_2-(o-H_2)$_n$ clusters with large n number should hardly appear with very low concentration of o-H_2. For instance, with 0.1% o-H_2 concentration in solid p-H_2, the statistical probability for the CO_2 molecules with one and two nearest neighbor o-H_2 molecules should be only 1.2% and 7×10^{-5}, respectively. However, it is obvious that the observed line intensities assigned to these clusters are much larger than expected. It provides evidence of the diffusion of the o-H_2 molecules in the solid molecular hydrogen. Such diffusion takes place with the exchange of the nuclear spins and rotational quanta between a pair of nearby p-$H_2\cdots o$-H_2 molecules. As given by Ran et al.,[24] the calculated potential energy of the $CO_2\cdots o$-H_2 complex is lower than that of $CO_2\cdots p$-H_2 by about 22 cm^{-1}. As a result, the doped CO_2 molecule would accumulate o-H_2 molecules in its inner solvent shell. As Figure 7 shows, with 25% o-H_2 concentration, the inner shell surrounding the CO_2 dopant is almost fully occupied with o-H_2 molecules.

The $CO_2\cdots(o\text{-}H_2)_n$ assignment is further confirmed with the spectrum we observed when some O_2 gas was mixed in the sample gas before deposition. Figure 8 shows the spectrum recorded with $CO_2/O_2/p$-H_2 sample just after deposition, 20 h later, and 120 h later. The O_2 concentration was 0.5% and the initial o-H_2 concentration was about 0.1%. As shown in the figure, beside the new peaks observed around 2344.6 cm^{-1} which can be readily assigned to the CO_2−O_2 clusters, the lines starting from 2343.9 cm^{-1}, which were assigned to $CO_2\cdots(o\text{-}H_2)_n$ (n = 1, 2, 3, etc.)

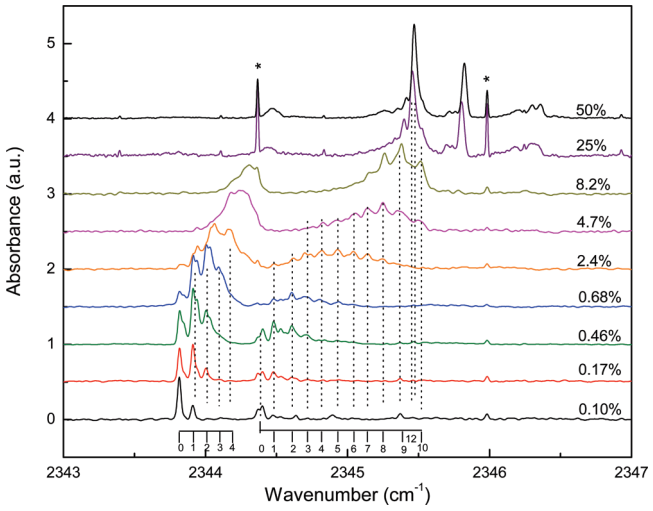

Figure 7. The ν_3 band of $^{12}C^{16}O_2$ isolated in solid hydrogen with different ortho-hydrogen concentration in the matrix (4.4 K). The lines marked with "*" are due to gas-phase CO_2 in the interferometer chamber. The index 1, 2, etc. shown on the figure indicates the number of o-H_2 molecules in the nearest neighbor of the doped CO_2 molecule.

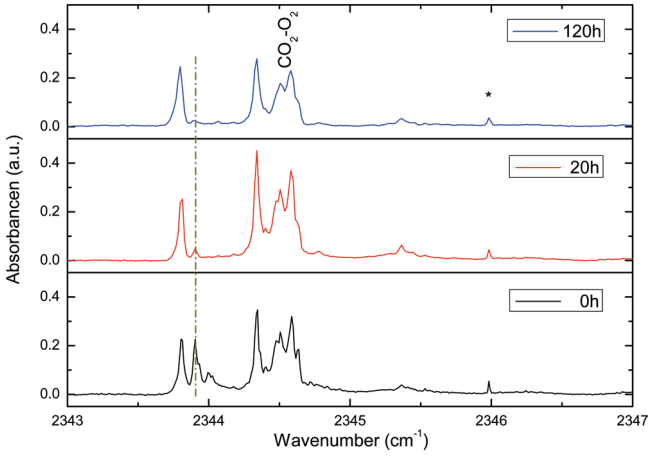

Figure 8. The ν_3 band of $^{12}C^{16}O_2$ isolated in solid para-hydrogen with 0.5% O_2. From bottom to top, three panels show the spectrum recorded just after deposition, 20 h later, and 120 h later, respectively. The lines marked with "*" are due to gas-phase CO_2 in the interferometer chamber, and the peaks around 2344.6 cm^{-1} are assigned to the CO_2-O_2 clusters in the p-H_2 matrix.

clusters, disappeared after several tens of hours after the deposition. As reported by Abouaf-Marguin et al., the doped paramagnetic O_2 molecule can work as effective catalyst to transfer o-H_2 to p-H_2 in the solid hydrogen.[4] In the present experiment, the presence of O_2 led to the slow decrease of the o-H_2 concentration in the matrix, which resulted in the decreasing of the transitions from the $CO_2\cdots(o\text{-}H_2)_n$ clusters. We have measured the o-$H_2 \Rightarrow p$-H_2 conversion rate in the O_2 doped solid molecular hydrogen in a separate experiment, which gives about $(15\ h)^{-1}$. Such a conversion rate also agrees well with the results presented in Figure 8.

With high o-H_2 concentration, some new lines come out at the higher frequency region over 2345 cm^{-1} in the case of $^{12}C^{16}O_2$. These lines are also reversible when the temperature changes. As discussed earlier, since the doped CO_2 molecule can attract o-H_2 molecules, the nearby p-H_2 molecules will be fully substituted with o-H_2. This is why the spectrum becomes clean again and does not change when the o-H_2 concentration is further increased. The new blue-shifted lines are thus assigned to the energy splitting because of different alignments of the CO_2 molecule in a solid o-H_2 matrix. The energy-splitting mechanism should be similar to that which has been discussed for the p-H_2 matrix.

5. CONCLUSION

The spectrum of the ν_3 band in solid H_2 exhibits rich spectral structures. Simulation of the potential energy of the CO_2 molecule doped in para-hydrogen matrix was carried out on the basis of the two-body CO_2-H_2 potential. It shows that the CO_2 rotation is hindered by the solid H_2 matrix, but there will be considerable tunneling between different orientations of the CO_2 molecule in the matrix. Different groups of spectral lines are observed reversible and sensitive to the temperature, and the relaxation time of the spectral feature is hours long at 4 K but much shorter at 5 K. We propose to attribute it as a result of energy level splitting because of tunneling between different alignments of the doped CO_2 molecules in the matrix. The temperature dependence can be interpreted as the change of the population distribution of different orientations of CO_2 in the matrix when the temperature changes. However, it is still hard to give a quantitative interpretation without further theoretical and computational studies.

On the basis of the observation carried out with different ortho-hydrogen concentrations in the matrix, the fine spectral features are assigned to the $CO_2\cdots(o\text{-}H_2)_n$ clusters. The assignments are supported with the experiments recorded with different CO_2 isotopologues and also with that obtained with codoped O_2 in the matrix. The matrix shift analysis of the spectra observed with different isotopologues also reveals that some nearby H_2 molecules may be kinetically involved in the stretching vibrations of the doped CO_2 molecule.

Study of the spectrum of solid hydrogen doped with molecules like CO_2 can potentially provide rich dynamics of molecular system with only very weak van der Waals interactions involved. Further theoretical and experimental investigations will continuously supply more quantitative information and deeper understanding of the dynamics in this interesting system. Since trace CO_2 often presents as a minor contamination in the sample when studying solid hydrogen, the CO_2 ν_3 band spectra presented in this work will also provide an alternative way to characterize the solid hydrogen matrix, such as to determine the temperature and the o-H_2 concentration in the solid molecular hydrogen.

AUTHOR INFORMATION

Corresponding Author

*E-mail: smhu@ustc.edu.cn.

ACKNOWLEDGMENT

The authors are indebted to Dr. M.-C. Chan from CUHK for numerous helpful suggestions and discussions. Dr. F. Qi in NSRL is acknowledged for PIMS mass spectroscopy measurements. Dr. V. I. Perevalov (IAO, Tomsk) is acknowledged for discussion on the vibrational states of CO_2. This work is jointly supported by NSFC(20903085, 20873132, 10728408), by

FRFCU(WK2340000012) and by NKBRSF(2006CB22001, 2007CB815203).

REFERENCES

(1) Tam, S.; Fajardo, M. E.; Katsuki, H.; Hoshina, H.; Wakabayashi, T.; Momose, T. *J. Chem. Phys.* **1999**, *111*, 4191–4198.
(2) Katsuki, H.; Momose, T. *Phys. Rev. Lett.* **2000**, *84*, 3286–3289.
(3) Fajardo, M. E.; Tam, S.; DeRose, M. E. *J. Mol. Struct.* **2004**, *111*, 695–696.
(4) Abouaf-Marguin, L.; Vasserot, A. M.; Pardanaud, C.; Stienlet, J.; Michaut, X. *Chem. Phys. Lett.* **2008**, *454*, 61–64.
(5) Fajardo, M. E.; Lindsay, C. M.; Momose, T. *J. Chem. Phys.* **2009**, *130*, 244508.
(6) Anderson, D. T.; Hinde, R. J.; Tam, S.; Fajardo, M. *J. Chem. Phys.* **2002**, *116*, 594.
(7) Paulson, L. O.; Anderson, D. T. *J. Phys. Chem. A* **2009**, *113*, 1770–1778.
(8) Yoshioka, K.; Anderson, D. T. *J. Chem. Phys.* **2003**, *119*, 4731–4742.
(9) Abrouaf-Marguin, L.; Vasserot, A. M.; Lekic, A. *Chem. Phys. Lett.* **2009**, *470*, 228–232.
(10) Lee, Y.-P.; Wu, Y.-J.; Hougen, J. T. *J. Chem. Phys.* **2008**, *129*, 104502.
(11) Raston, P. L.; Kettwich, S. C.; Anderson, D. T. *Low Temp. Phys.* **2010**, *36*, 392–399.
(12) Lorenz, B. D.; Anderson, D. T. *J. Chem. Phys.* **2007**, *126*, 184506.
(13) Hu, S.-M.; Wan, L.; Du, J.-H.; Xu, G.; Deng, W.-P.; Wu, L.; Tian, S.-X.; Chen, Y. *Vib. Spectrosc.* **2009**, *50*, 36–42.
(14) Schriver, A.; Schriver-Mazzuoli, L.; Vigasin, A. A. *Vib. Spectrosc.* **2000**, *23*, 83–94.
(15) Castano, J.; Fantoni, A.; Romano, R. *J. Mol. Struct.* **2008**, *881*, 68–75.
(16) Minenko, M.; Vetter, M.; Brodyanski, A. P.; Jodl, H. J. *Low Temp. Phys.* **2000**, *26*, 699–711.
(17) Wan, L.; Xu, G.; Wu, L.; Chen, Y.; Hu, S.-M. *J. Mol. Spectrosc.* **2009**, *257*, 217–219.
(18) Nxumalo, L. M.; Ford, T. A. *J. Mol. Struct.* **1994**, *327*, 145–159.
(19) Loewenschuss, A.; Givan, A. *Spectrosc. Lett.* **1977**, *10*, 551–558.
(20) Tam, S.; Fajardo, M. *Low Temp. Phys.* **2000**, *26*, 653–660.
(21) Nauta, K.; Miller, R. *J. Chem. Phys.* **2001**, *115*, 10254–10260.
(22) McKellar, A. R. W. *J. Chem. Phys.* **2005**, *122*, 174313.
(23) Wang, L.; Yang, M.; McKellar, A. R. W.; Zhang, D. H. *Phys. Chem. Chem. Phys.* **2007**, *9*, 131–137.
(24) Ran, H.; Zhou, Y.; Xie, D. *J. Chem. Phys.* **2007**, *126*, 204304.
(25) Ralph, E. M.; Decius, J. C. *J. Chem. Phys.* **1973**, *59*, 4871–4883.
(26) Deng, W.-P.; Xu, G.; Wan, L.; Liu, A.-W.; Gao, B.; Du, J.-H.; HU, S.-M.; Chen, Y. *Acta Phys. Chim. Sin.* **2008**, *24*, 1329–1334.
(27) Fajardo, M.; Tam, S. *J. Chem. Phys.* **1998**, *108*, 4237–4241.
(28) Teffo, J. L.; Claveau, C.; Valentin, A. *J. Quant. Spectrosc. Radiat. Transfer* **1998**, *59*, 151–164.
(29) Rothman, L. S.; et al. *J. Quant. Spectrosc. Radiat. Transfer* **2005**, *96*, 139–204.
(30) *Molecular Spectra and molecular structure*; Herzberg, G., Ed.; D. Van Nostrand Company: New York, 1945.